α-particle stopping cross section of gold and silver as measured from thick targets*

W. K. Lin,† S. Matteson, and D. Powers
Baylor University, Waco, Texas 76703
(Received 3 June 1974)

Stopping cross sections of α particles in Au and Ag have been obtained for $0.3 \leq E_\alpha \leq 2.0$ MeV. The experimental method consists of measuring the energy spectra of α particles elastically scattered from thick targets. The experimental details as well as the method for extracting the stopping cross section from measured energy spectra are discussed. The results are found to be in good agreement with those previously obtained using thin targets.

I. INTRODUCTION

The measurement of the stopping cross section $\epsilon = -dE/Ndx$ usually requires the determination of both the number of stopping atoms per unit area $N\Delta x$, and the corresponding energy loss ΔE to the moving charged particle. In the work reported by Chu and Powers[1] and recently by Lin *et al.*,[2,3] a thin film of the solid stopping element was prepared by vacuum evaporation within a known area onto a Ta or Al backing. $N\Delta x$ was obtained from the weight of the target element deposited on the area. The energy loss ΔE was related kinematically to the difference in energies of the α particles scattered by Ta atoms on the front surface of a clean Ta blank and on another blank onto which the target element had been evaporated. For the stopping elements whose atomic weights are significantly greater than that of Al, an Al backing was also used. In this case, however, the determination of ΔE was made from the difference in energies of α particles scattered by the target atoms on the front and back surfaces of the target film. On many occasions, it becomes rather difficult to prepare a thin film by vacuum evaporation and to determine its corresponding $N\Delta x$ by weighing. Chemically reactive elements oxidize readily in the weighing process; laborious radiation safety precautions are required for evaporation of the radioactive element; and the crystal structure usually cannot be preserved when the stopping element is being vapor-deposited on some substrates.

This work was undertaken to measure the α-particle stopping cross sections of Au and Ag from thick targets. The thick-target method avoids the necessity for a determination of $N\Delta x$, and was used previously by Wenzel and Whaling[4] in their measurement of the proton stopping cross section of ice. The energy spectrum of protons elastically scattered by the oxygen atoms in ice was obtained by a double-focusing magnetic spectrometer, whose angular and energy resolution were accurately known. In the present work, a surface-barrier counter was used instead to record the α-particle energy spectrum. The thick-target method was found to be quite efficient, when due precaution was taken for charge collection, energy calibration, and dead-time effects. The reason for choosing Au and Ag to start with is that they are chemically stable and easily prepared by vacuum evaporation. The properties of gold films on solid substrates are of great technological importance; the determination of these properties requires a reliable stopping-cross-section measurement of Au, if the backscattering technique is to be used. The α-particle stopping cross section of Au has been recently remeasured by Borders[5] and by Lin *et al.*[2] using thin targets. Although their error bars overlapped, the data given in Ref. 5 appeared to be systematically lower than data given in Ref. 2. The results of the present work offer an additional independent check to those measurements.

II. EXPERIMENTAL METHOD

When an α particle of energy $E_\alpha = E_{10}$ traverses a thick target at an angle θ_1 with respect to the normal to the target surface, it slows down and may also encounter scattering by the stopping atoms. Let E_{1S} and E_{2S}, respectively, be the α-particle energies just before and after scattering at a laboratory angle θ and depth S beneath the target surface. The scattered α particle will continue to be slowed down before it emerges from the target. In the continuous slowing-down approximation (csda),[6] the energy E_{20} of the detected α particles is related to the incident energy E_{10} by

$$S \sec\theta_1 = \frac{1}{N}\int_{E_{1S}}^{E_{10}} \frac{dE}{\epsilon(E)} \quad ,$$

and

$$S \sec\theta_2 = \frac{1}{N}\int_{E_{20}}^{E_{2S}} \frac{dE}{\epsilon(E)} \quad ,$$

where $\theta_2 = \pi - \theta - \theta_1$ and N is the number of stopping atoms per unit volume. The stopping cross

section $\epsilon(E)$ as a function of particle energy is to be determined. By differentiation of these integrals, one obtains the following two useful relationships,

$$\frac{dS}{dE_{20}} = -\frac{\epsilon(E_{2S})\cos\theta_1}{N\epsilon(E_{20})[\alpha\epsilon(E_{1S})+\beta\epsilon(E_{2S})]} \quad (1)$$

and

$$\frac{dE_{1S}}{dE_{20}} = \frac{\epsilon(E_{1S})\epsilon(E_{2S})}{\epsilon(E_{20})[\alpha\epsilon(E_{1S})+\beta\epsilon(E_{2S})]}\ , \quad (2)$$

where $\beta = \cos\theta_1/\cos\theta_2$ and the kinematic factor α describing scattering of α particles of mass M_α by stopping atoms of mass M is

$$\alpha = \frac{dE_{2S}}{dE_{1S}} = \left(\frac{M_\alpha\cos\theta + (M^2 - M_\alpha^2\sin^2\theta)^{1/2}}{M_\alpha + M}\right)^2 .$$

The scattering yield per unit energy interval can be written with the use of expression (1) as

$$y(E_{10}, E_{20}) = N_b\Delta\Omega\frac{d\sigma}{d\Omega}\frac{N}{\cos\theta_1}\left|\frac{dS}{dE_{20}}\right|$$
$$= N_b\Delta\Omega\frac{d\sigma}{d\Omega}\frac{\epsilon(E_{2S})}{\epsilon(E_{20})[\alpha\epsilon(E_{1S})+\beta\epsilon(E_{2S})]} . \quad (3)$$

N_b and $\Delta\Omega$ are, respectively, the number of incident α particles and the solid angle subtended by the detector. The scattering cross section $d\sigma/d\Omega$ is understood to be a function of E_{1S} and θ. As has been demonstrated by Smith *et al.*[7] and Wijngaarden *et al.*,[8] the scattering of α particles by the target atom, at an energy well below the Coulomb barrier, can be accurately described by the classical scattering from a shell-shielded Coulomb potential, with a screening distance d equal to two times the Thomas-Fermi parameter. The corresponding scattering cross section has a simple analytic expression as

$$\frac{d\sigma}{d\Omega} = \left(\frac{d\sigma}{d\Omega}\right)_R\left(\frac{1+b/2d}{1+(b/d)+b^2/4d^2\sin^2\frac{1}{2}\theta_c}\right)^2 , \quad (4)$$

where $b = Z_\alpha Ze^2(1+M_\alpha/M)/E_{1S}$, with Z_α and Z representing the atomic number of the α particle and the target atom, is the distance of closest approach in a head-on collision. The Rutherford cross section $(d\sigma/d\Omega)_R$ and the factor $\sin^2\frac{1}{2}\theta_c$ are expressed in terms of the laboratory scattering angle θ, respectively, as

$$\left(\frac{d\sigma}{d\Omega}\right)_R = \frac{Z_\alpha^2Z^2e^4}{4E_{1S}^2\sin^4\theta} \times\frac{[M\cos\theta+(M^2-M_\alpha^2\sin^2\theta)^{1/2}]^2}{M(M^2-M_\alpha^2\sin^2\theta)^{1/2}}$$

and

$$\sin^2\tfrac{1}{2}\theta_c = [(M_\alpha+M)/2M](1-\alpha^{1/2}\cos\theta) .$$

The classical scattering cross section derived from the shell-shielded Coulomb potential was used although it deviated from the Rutherford scattering cross section by less than 3% in the energy range of interest. The magnetically analyzed He^+ beam (typically ~100 nA) from a 2-MV Van de Graaff accelerator was collimated to a 1.6-mm square before striking the target. The α particles elastically scattered at $\theta = 130°$ were detected by a 100-μm surface-barrier counter, collimated by a circular aperture of 13.7-mm diameter, 13.8 cm from the beam spot. Figure 1 shows the detection

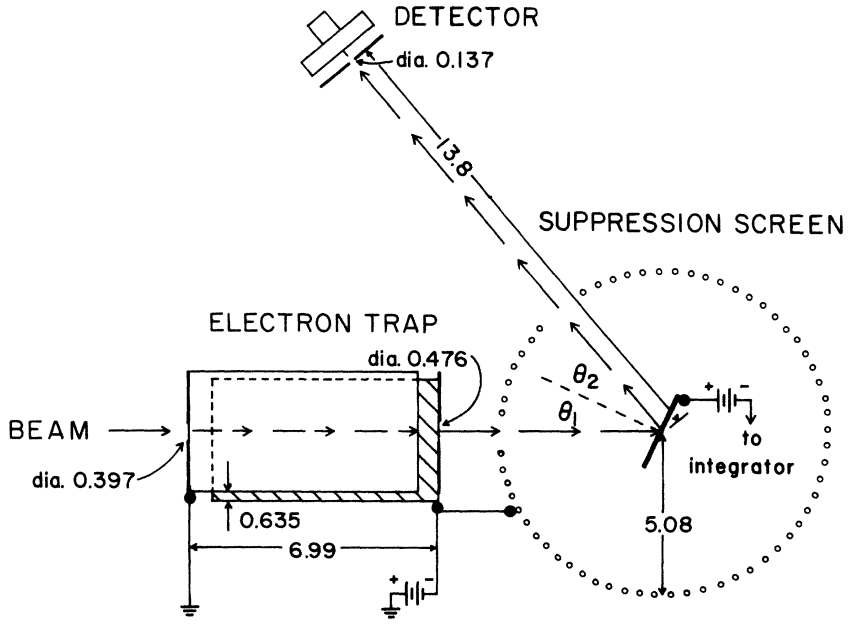

FIG. 1. Detection geometry and electron suppression system. The electron trap consists of two parallel plates with one grounded and the other biased at −450 V. The electric field is perpendicular to the plane of the figure. The target rod and the electron suppression screen, shown as a dotted circle, are, respectively, held at + and −450 V. The laboratory scattering angle $\theta = 130°$ is equal to $\pi - \theta_1 - \theta_2$, where $\theta_1 = \theta_2 = 25°$ are the angles, respectively, of the incident and detected α particles with respect to the normal to the target surface.

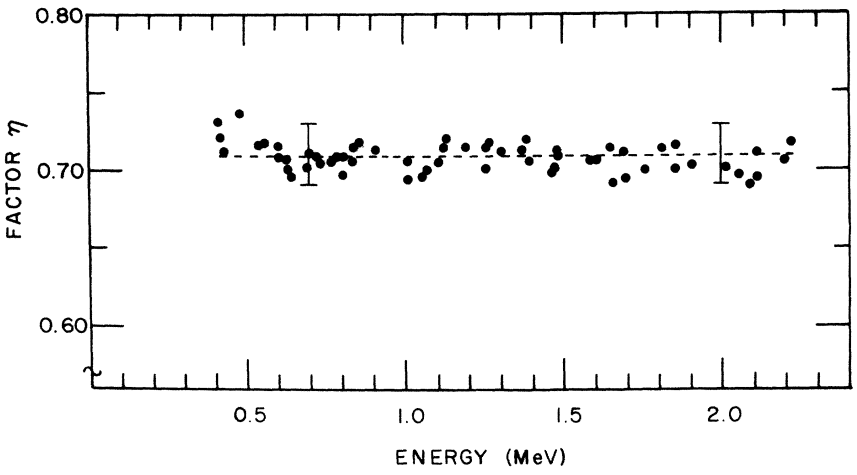

FIG. 2. Calibration of the current integrator. The factor η is equal to the measured scattering yield from a reference thin target of known areal density divided by the yield calculated by taking the total charge from the current integrator reading, Q. The number of incident α particles which strike the target during the run times the solid angle subtended by the detector, represented by the product $N_b\Delta\Omega$, is related to η and Q by expression (5). The dashed line is the mean of all the measured values and the error bars correspond to the $\pm 3\%$ deviation from the mean value.

geometry and the arrangement of the electron suppression system. The electron trap, consisting of a grounded plate 6.35 mm above the lower plate biased at -450 V, collected the secondary electrons produced by the beam-collimating slits. The same negative voltage was also applied to the cylindrical suppression screen of 5.08-cm diameter to help prevent the secondary electrons generated at the target from escaping. The target rod itself was held at $+450$ V above the ground. An Elcor current integrator was used to monitor the total charge that accumulated from a He^+ beam on the target during the run. An absolute calibration of the integrator would be necessary if N_b were measured this way. An alternate procedure was used instead, which involved the measurement, under the same experimental condition with which a thick-target spectrum was taken, of the scattering yield from the bombardment of a thin Au or Ag target of known $N\Delta x$. The reference thin target was, typically, 60 $\mu g/cm^2$ thick and involved a maximum energy loss of 27 keV in the target based on previously measured stopping powers of Au or Ag. The thin target was arbitrarily divided into 50 small layers of equal thickness, the mean energy in each layer was calculated, and the reference-thin-target yield was obtained by summing the yields from each of the 50 layers in the target. The ratio of this scattering yield to that calculated by assuming the total charge to be indicated by the current integrator is given by a factor η which is plotted in Fig. 2. This factor η was found to be fairly constant within $\pm 3\%$ for $0.4 \leq E_\alpha \leq 2.2$ MeV, and was also found to be quite insensitive to the value of the Au or Ag stopping power used in calculating the mean energy in each of the 50 layers into which the reference thin target was subdivided. The product $N_b\Delta\Omega$ needed for expression (3) is thereby found to be

$$N_b\Delta\Omega = 6.148\times 10^8 \eta Q \ , \qquad (5)$$

for the detection geometry used in this work. The quantity Q, expressed in μC, is the integrated charge as indicated by the current integrator. The importance of an accurate measurement of N_b and $\Delta\Omega$ in nuclear elastic scattering experiments is noted.[4,9]

The signal from the detector, through a preamplifier and a linear amplifier, was analyzed by a 50-MHz 256-channel analyzer. The output of the linear amplifier was branched to a single-channel analyzer. Pulses above a preset lower discrimination level were counted by a fast scaler and were also used to gate the multichannel analyzer. The total number of counts integrated from the analyzer spectrum divided by that counted by the scaler provided a reliable quantity for dead-time correction for the analyzing system. Since the energy E_{20} of expression (3) is always less than or equal to $E_{2B} = \alpha E_{10}$, the analyzer spectrum has a step at its high-energy end. The width of the step is due mainly to the detector resolution. The energy corresponding to channel number C_{2B} at the midpoint[2] of the step is identical to E_{2B}. The energy at any other channel in the spectrum can be determined by examining the similar spectra taken at neighboring bombarding energies. However, in order to use a suitable common amplifier gain for taking all the spectra at $0.4 \leq E_{10} \leq 2.0$ MeV, the input threshold and the digital offset of the multichannel analyzer had to be changed from the run taken at one value of E_{10} to another. To

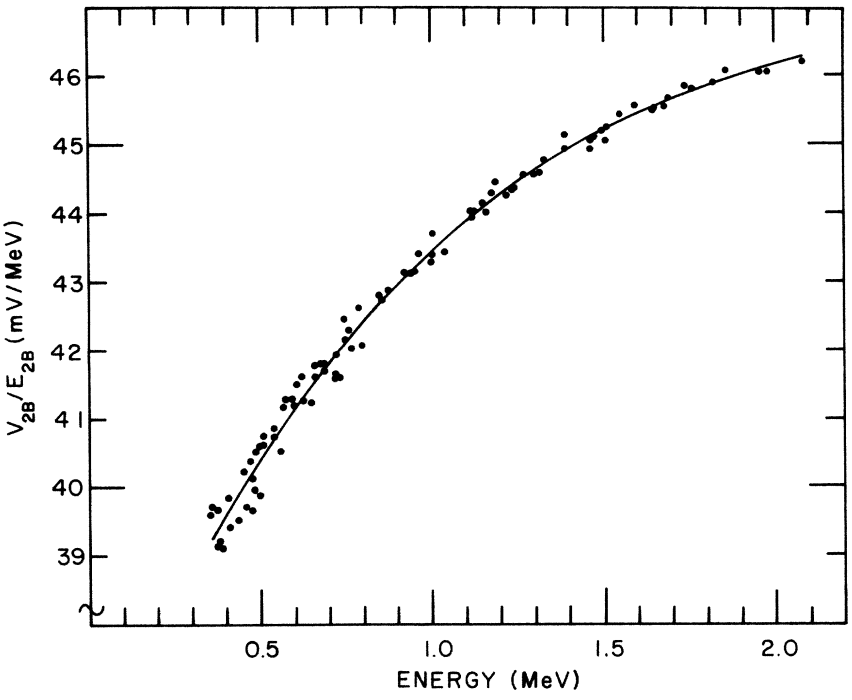

FIG. 3. Energy calibration for the surface-barrier counter. Three to five pulses of different voltage from a precision pulser were fed in through the preamplifier and analyzed in the multichannel analyzer. By doing so, one was able to determine the voltage per channel, dV/dC, and also the voltage V_{2B} corresponding to the midpoint of the high-energy step of each analyzer spectrum. Since the energy corresponding to V_{2B} is E_{2B}, the ratio V_{2B}/E_{2B} measures the linearity of the counter. The fact that the ratio deviates so much from a straight line indicates the effects due to the dead layer and other pulse-height defect mechanisms in the surface-barrier detector. The result obtained from fitting the data points to a third-degree polynomial of energy is shown by the curve, from which the energy per unit voltage interval, dE/dV, was derived. The energy per channel, $dE/dC = (dE/dV)(dV/dC)$, was then computed.

facilitate the energy calibration, three to five pulses of different voltage from a precision pulser were fed through the preamplifier and analyzed every time after a spectrum was taken. The voltage per channel, dV/dC, and thus the voltage V_{2B} corresponding to channel number C_{2B} were computed. Figure 3 shows the ratio V_{2B}/E_{2B} obtained for different energies. The fact that it changes by about 15% over the entire energy range indicates the importance of effects due to the dead layer and other pulse-height defect mechanisms of a surface-barrier counter. A third-degree polynomial curve fit was made to the measured values of V_{2B}/E_{2B} in Fig. 3. From this curve the energy per voltage interval dE/dV and subsequently the energy per channel $dE/dC = (dE/dV)(dV/dC)$ were determined. From this function dE/dC and the condition that $E = E_{2B}$ at $C = C_{2B}$, the analyzer spectrum containing the counts per channel can be readily transformed into the energy spectrum to represent the counts detected within an energy interval ΔE. Several of these energy spectra, which cover a larger energy range, are shown in Figs. 4 and 5.

III. DATA ANALYSIS

In addition to the detector resolution mentioned previously, both the energy straggling and multiple scattering may also cause fluctuations in α-particle energy. An energy spectrum to be represented by $Y(E_{10}, E_{20})$, such as one shown in Figs. 4 and 5, should be compared with expression (3) folded in with a response function which includes these effects. It will be shown in the development which follows, however, that by limiting the detected energy spectrum to energies E_{20} between $E_c \simeq \alpha E_{10} - 0.1$ MeV and $E_{2B} = \alpha E_{10}$, that both multiple scattering and energy straggling contribute small errors ($< 2\%$) to the scattering yield. The response function is thereby adequately represented by the Gaussian detection response function

$$Y_c(E_{10}, E_{20}) = \frac{\Delta E}{(2\pi)^{1/2}} \int \frac{1}{\delta(E)} \exp\left[-\frac{1}{2}\left(\frac{E_{20} - E}{\delta(E)}\right)^2\right] \times y(E_{10}, E)\, dE \,, \qquad (6)$$

where ΔE is now the unit energy interval used in the transformation of the analyzer spectrum to the

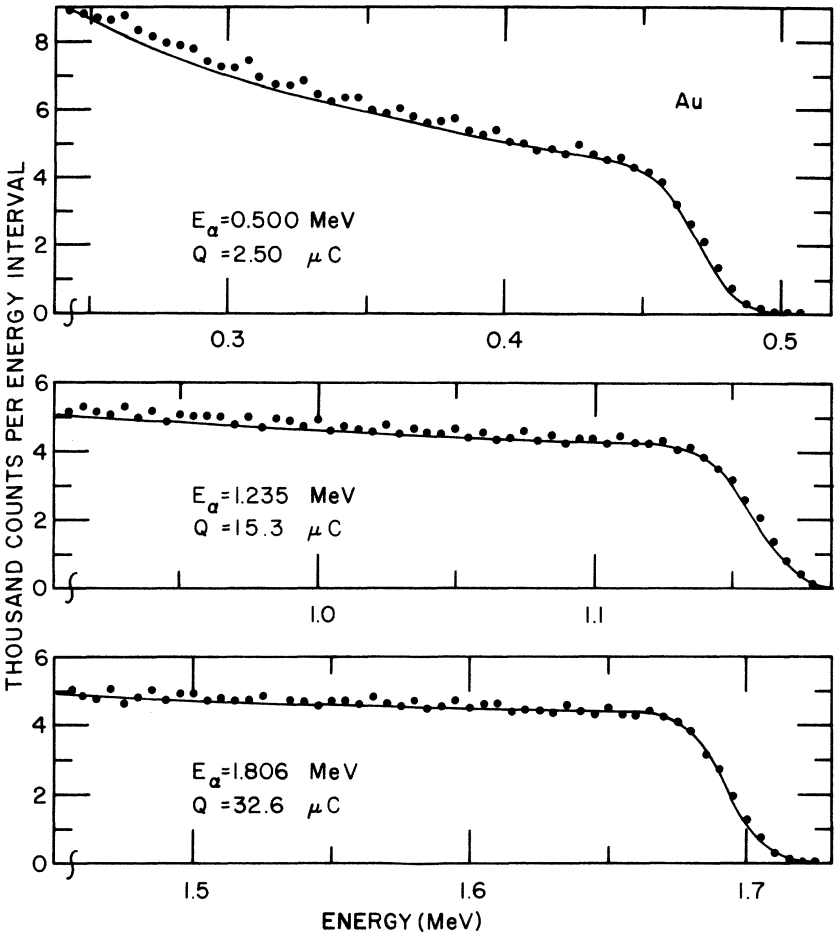

FIG. 4. Energy spectra from bombardment of α particles on thick Au targets. From a total of 43 spectra taken, the three shown cover the widest energy region. The transformation from the actual analyzer spectra to these spectra, representing the counts received in an energy interval of $\Delta E = 5$ keV, were carried out with the energy calibration shown in Fig. 3. E_α and Q, which label the spectrum are, respectively, the incident energy and the total charge indicated by the integrator. The curves Y_c were calculated using the stopping cross section generated by the parameters $(n, a, z) = (2.83, 0.337, 3.15)$. As discussed in the text, the amount of disagreement between the measured energy spectrum Y and the calculated energy spectrum Y_c for $E_\alpha = 0.5$ MeV is still within the error assigned for this work.

energy spectrum Y, and the variance δ is due to the finite detector resolution. As for multiple scattering, the α particle gradually diverges about its original direction in the stopping medium. The mean-square angle of divergence[10] is approximately proportional to a quantity equal to the α-particle energy loss due to the nuclear collisions divided by its initial energy. The root-mean-square angle of divergence, a measure of the uncertainty in angle at which the α particle is scattered, increases as the α particle penetrates deeper inside the target. Since both the scattering yield and the kinematic factor α are larger for smaller scattering angles, the energy fluctuation due to multiple scattering will deviate from the symmetric Gaussian distribution and cause an increase in the scattering yield, as the rms angle of divergence becomes sufficiently large. To avoid the possible complication owing to this increase in scattering yield, expression (6) was calculated only for the values of E_{20} between a cutoff energy $E_c \simeq \alpha E_{10} - 0.1$ MeV and $E_{2B} = \alpha E_{10}$ to compare with the corresponding part of the measured energy spectrum. The errors incurred were estimated for $E_{10} \geq 0.4$ MeV, using the results given in Ref. 8, to be less than 2% and 1% for Au and Ag, respectively.

The effect of energy straggling is to degrade the energy resolution of both incident and scattered α particles,[10] which may cause a noticeable increase or decrease in the yield for E_{20} values considerably less than $E_{2B} = \alpha E_{10}$. For target thicknesses contributing to the spectrum from E_{2B} to $E_c \simeq \alpha E_{10} - 0.1$ MeV, a simple calculation shows that energy straggling is not important. The recent energy straggling measurements of Harris *et al.*[11] for 1 to 2-MeV α particles in Pt ($Z = 78$) give a good approximation to the energy straggling in Au ($Z = 79$). For the geometry of the present experiment, their measurements predict a maximum energy straggling of approximately 5 keV, which when added in quadrature to the instrumental (detection system) resolution (typically 12–14 keV), gives a negligible contribution. Further evidence of the relative insignificance of both multiple scattering and energy straggling is seen in the remarkably close fits between calculated and observed spectra for a much larger energy spread in E_{20} than that used in the analysis of this paper.

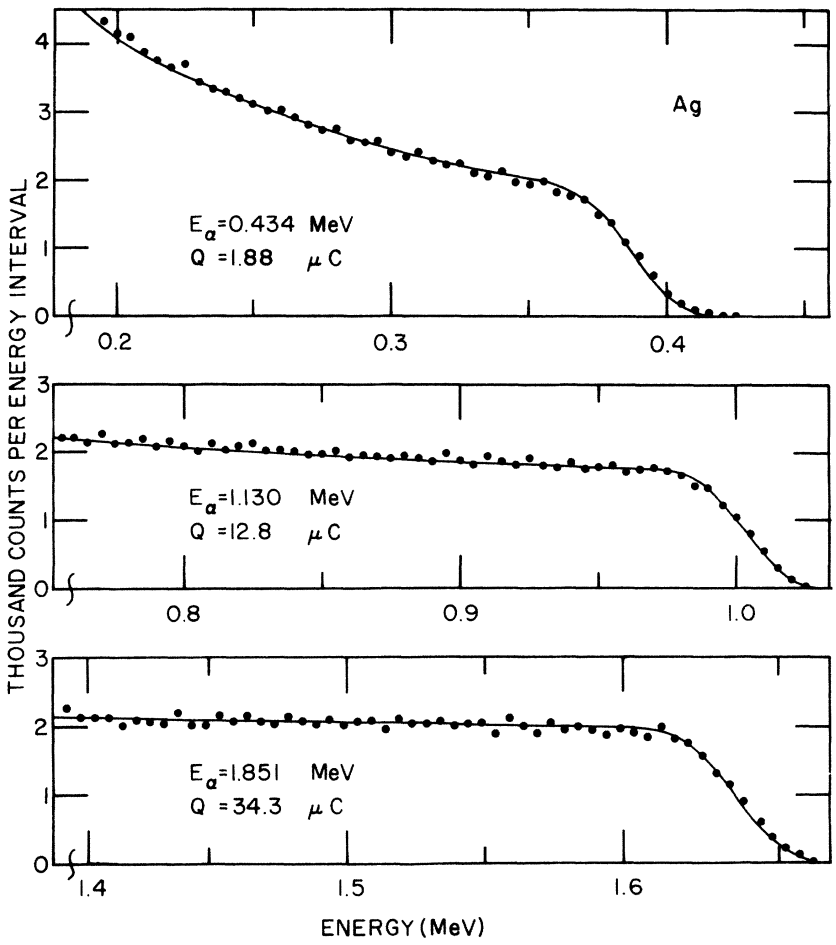

FIG. 5. Energy spectra from bombardment of α particles on thick Ag target. (see the caption for Fig. 4). The curves were calculated using the stopping cross section of Ag with the parameters $(n, a, z) = (3.10, 0.352, 2.32)$.

The spectra of Figs. 4 and 5, for example, cover an energy spread in E_{20} from $\simeq E_{2B} - 0.3$ MeV to E_{2B} (three times greater than that actually used in the analysis), and yet the deviation between calculated and observed spectrum at $E_{20} \simeq E_{2B} - 0.3$ MeV is still typically < 3%. Consequently, multiple scattering and energy straggling contribute a negligible effect to the values of stopping cross sections of Au and Ag obtained by the present experimental method.

As can be seen from expression (3), the function $y(E_{10}, E)$ appearing in the integrand of expression (6) varies very slowly over the energy region required for the integration. The calculated energy spectrum Y_c therefore turns out to be not very sensitive to any slow energy dependence of δ. In this analysis, the integration in expression (6) was considerably simplified by assuming a constant value of δ, which was determined for each spectrum by fitting the high-energy end of the energy spectrum to the expression. For this purpose $y(E_{10}, E)$ was taken to be a linear function of E.

To extract the stopping cross section ϵ, it was found[2,3] convenient to parameterize ϵ by a formula given by Brice[12] as

$$\epsilon = \frac{4\hbar^2}{5m} \frac{Z_\alpha + Z}{1 + (av/v_0)^n} \left(x^{1/2} \frac{30x^2 + 53x + 21}{3(x+1)^2} + (10x+1)\tan^{-1}x^{1/2} \right), \quad (7)$$

where $x = (v/2v_0z)^2$, $v_0 = e^2/\hbar$, and the α-particle velocity and the electronic mass are denoted by v and m, respectively. The formula contains three parameters, namely n, a, and z, and has been shown[2,3,12] to fit α-particle stopping cross sections for 0.3–2.0 MeV for a variety of substances to better than 3%. With the product $N_b \Delta\Omega$ and the scattering cross section $d\sigma/d\Omega$, respectively, given by expressions (5) and (4), the function $y(E_{10}, E_{20})$ for a given set of these parameters can be evaluated from formula (7) as a function of E_{20}, once the energies E_{1S} and thus $E_{2S} = \alpha E_{1S}$ are determined. From the initial condition that $E_{1S} = E_{10}$ and $E_{20} = E_{2B}$, the value for E_{1S} corresponding to other values of E_{20} was obtained by solving numerically the differential equation (2). The stopping cross section was obtained by first determining the set of parameters which minimized the

TABLE I. Stopping cross sections of Ag and Au for α particles.

Energy (MeV)	Ag $dE/\rho\,dx$ (keV cm^2/μg)	Ag ϵ (10^{-15} eV cm^2)	Au $dE/\rho\,dx$ (keV cm^2/μg)	Au ϵ (10^{-15} eV cm^2)
0.3	0.502	89.8	0.306	100.2
0.4	0.555	99.3	0.335	109.7
0.5	0.589	105.5	0.354	116.0
0.6	0.610	109.3	0.366	119.9
0.7	0.622	111.4	0.374	122.3
0.8	0.627	112.2	0.377	123.5
0.9	0.627	112.2	0.379	124.0
1.0	0.623	111.5	0.378	123.8
1.1	0.617	110.5	0.376	123.2
1.2	0.609	109.1	0.374	122.4
1.3	0.601	107.6	0.371	121.3
1.4	0.591	105.9	0.367	120.1
1.5	0.582	104.2	0.363	118.8
1.6	0.572	102.5	0.359	117.5
1.7	0.562	100.7	0.355	116.1
1.8	0.552	99.0	0.350	114.7
1.9	0.543	97.3	0.346	113.3
2.0	0.534	95.6	0.342	112.0

quantity

$$F=\sum_{j=1}^{J}\int_{E_c}^{E_{2B}}[Y(E_j,E_{20})-Y_c(E_j,E_{20})]^2\,dE_{20}\,, \quad (8)$$

where $E_{2B}=\alpha E_j$, with j labeling the energy $E_{10}=E_j$ at which the energy spectrum Y was measured and the calculated energy spectrum Y_c was made. The cutoff energy E_c, as has been explained, was taken to be around $E_{2B}-0.1$ MeV. The total number of spectra J included in the least-squares fitting is 43 (40) for Au (Ag). To simplify the minimization procedure for expression (8), the function $y(E_j,E)$ in expression (6) for the evaluation of $Y_c(E_j,E_{20})$ was written as

$$y(E_j,E)\big|_{n,a,z}=y(E_j,E)\big|_{n_0,a_0,z_0}+(n-n_0)\frac{\partial y}{\partial n_0}$$

$$+(a-a_0)\frac{\partial y}{\partial a_0}+(z-z_0)\frac{\partial y}{\partial z_0}$$

in terms of the function and its partial derivatives with respect to the parameters, evaluated at a starting set of values n_0, a_0, and z_0. The vector $(n-n_0, a-a_0, z-z_0)$, determined by the standard method of the linear least-squares fit[13] plus the starting set (n_0, a_0, z_0), gave a new set of parameters. The solution was then iterated until it became stationary. The parameters corresponding to the final solution were $n=2.83$ (3.10), $a=0.337$ (0.352), and $z=3.15$ (2.32) for Au (Ag). The stopping cross sections obtained from these parameters are tabulated in 0.1-MeV intervals in Table I.

The stopping cross sections calculated from these parameters by using formula (7) are compared with the results obtained from thin-target measurements[1,2,5,14–16] in Figs. 6 and 7. Perhaps it is worthwhile to mention again that the present stopping cross section was derived from a total of more than 40 measured energy spectra. If one assumed that the stopping cross section suitable to describe each individual spectrum was instead equal to that shown in Figs. 6 or 7 multiplied by a constant, the constant could be easily determined for each spectrum from a simpler procedure than the least-squares fit. In so doing one determines the stopping cross section necessary to predict correctly each individual spectrum. The rms deviation of the constant of multiplication from unity was found to be less than 3% for both Au and Ag.

The curves shown in Figs. 4 and 5, along with the measured energy spectra, represent the calculated energy spectra using the above-mentioned parameters corresponding to the final solution to the minimization of expression (8). Even though the minimization was restricted only to an interval of 100 keV in the high-energy ends of the spectra, the calculation actually predicted quite well larger portions of the spectra. The 0.5-MeV measured spectrum for Au shown in Fig. 4 was higher than the calculated one by about 3% in the energy interval $E_c \le E_{20} \le E_{2B}$, and it may be tempting to attribute this discrepancy to the increase in scattering yield from multiple scattering or energy straggling, which had not been corrected for in the calculation. However, since the factor η, which appears in expression (5) and is shown in Fig. 2, was only determined within $\pm 3\%$, the discrepancy shown in the 0.5-MeV spectrum is still consistent

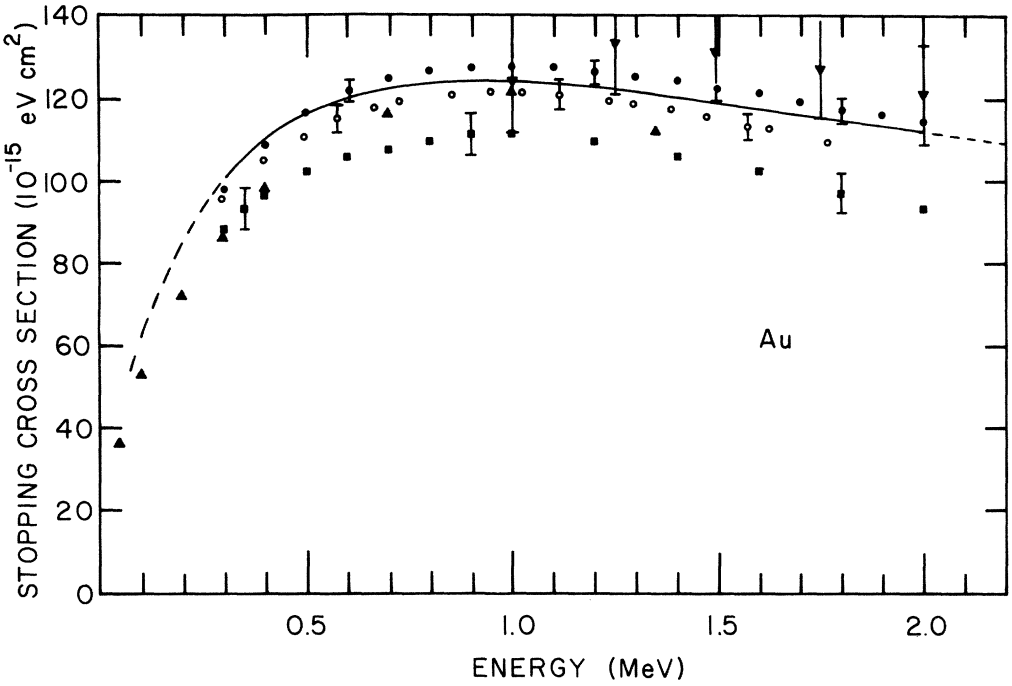

FIG. 6. Stopping cross section of α particles vs energy in Au. The solid curve and the extended dashed portions were calculated from formula (7) using the parameters $(n, a, z) = (2.83, 0.337, 3.15)$. These parameters were obtained from a total of 43 energy spectra of the type shown in Fig. 4 by minimizing the quantity given by expression (8). The results from thin-target measurements by Lin *et al.* (Ref. 2), Borders (Ref. 5), Porat and Ramavataram (Ref. 15), Gobeli (Ref. 14), and Allison and Warshaw (Ref. 16) are included for comparison. They are shown by closed circles (●), open circles (○), squares (■), inverted triangles (▼), and triangles (▲), respectively.

with the accuracy one could assign to this work.

IV. DISCUSSION

The experimental uncertainties which limit the accuracy of our measurements can be traced to the various quantities which have entered into the evaluation of expressions (3) and (6). Because we were able to fit simultaneously many spectra with the stopping cross section generated by expression (7) with the final set of three parameters only, the use of expression (4) for the scattering cross

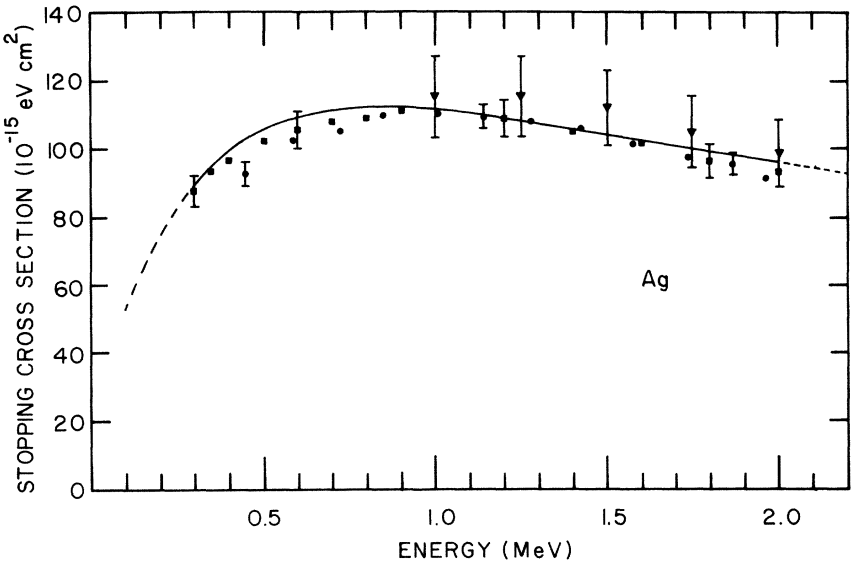

FIG. 7. Stopping cross section of α particles vs energy in Ag. The solid curve and its extended dashed portions were calculated from formula (7) using the parameters $(n, a, z) = (3.10, 0.352, 2.32)$. These parameters were obtained from a total of 40 energy spectra of the type shown in Fig. 5 by minimizing the quantity defined by expression (8). The results from thin-target measurements by Chu and Powers (Ref. 1), Porat and Ramavataram (Ref. 15), and Gobeli (Ref. 14) are included for comparison. They are given by closed circles (●), squares (■), and inverted triangles (▼), respectively.

section and the assumption for a constant value of δ for each spectrum taken at E_{10} in expression (6) appeared to be quite adequate. Judging also from the good agreement obtained in the energy dependence of the measured and calculated energy spectra, one might be able to relax somewhat the restriction imposed on comparing only the 100-keV high-energy ends of the spectra. It is possible that the results of Ref. 7, given for the calculation of the increase in scattering yield owing to multiple scattering for $E_{10} \leq 150$ keV, could have overestimated the effect when the results were applied to the energy region $E_{10} \geq 400$ keV. In taking the spectra at lower bombarding energies, because of the increase in the scattering cross section, the beam intensity was reduced to keep the dead time of the multichannel analyzer always less than 10%. Since no appreciable pulse pileup was observed and the fast scaler was capable of handling even much higher counting rates than we had encountered, the dead time of the entire pulse-analysis system is therefore dictated by that of the multichannel analyzer. Thus it was sufficient to use the ratio of counts from the fast scaler to the counts integrated from the analyzer spectrum for deriving our dead-time correction. The accuracy associated with the transformation of analyzer spectrum to the energy spectrum depended critically on the energy calibration. As shown in Fig. 3, we had taken into account the effects due to the dead layer and other pulse-height defect mechanisms in the surface-barrier counter by determining the amount of energy corresponding to unit voltage interval dE/dV from a considerable number of data points for the ratio V_{2B}/E_{2B}. From this dE/dV, as a function of energy, and the measured voltage per channel dV/dC in the analyzer, the energy calibration for the spectra was made to better than 1%.

An uncertainty arises from the determination of the product $N_b \Delta\Omega$, which as indicated by expression (5) is proportional to η. The factor η, shown in Fig. 2, is equal to the measured scattering yield from a reference thin target of known areal density $N\Delta x$ divided by the scattering yield calculated by taking the total integrated charge to be that indicated by the current integrator. The thin targets (typically ~60 μg/cm^2) were prepared on an Al substrate, and the scattering yield was determined from the analyzer spectrum by separating the scattering events due to target atoms from those due to the substrate atoms. Uncertainty may be introduced in this separation in case of low bombarding energy and greater areal density. In this respect a reference target of less thickness would be preferable; however being thinner, the less accurate one could determine its $N\Delta x$. Since the amount of α-particle energy loss in the target is small and the stopping cross section is always a slowly varying function of particle energy, the accuracy of the stopping cross section used for the energy-loss correction in the calculation of scattering yield is not important. In fact, the result was found to change less than 1%, for the bombarding-energy range of interest, even if the stopping cross section was purposely increased or decreased by 10%. Thus, the uncertainty in the factor η arose primarily from error in determining the thickness of the reference thin target. Taking the spread in the factor η observed in Fig. 2, together with the spread of 3% in stopping cross section obtained from spectrum-by-spectrum analysis, and the much smaller probable errors due to scattering cross section (< 1.5%; see Ref. 4), curve fitting (see data analysis), calibration (< 1%), energy straggling (< 1%), and multiple scattering effects (< 2%), we have assigned a probable error of 4% to our stopping cross sections.

It happens that the stopping cross sections of α particles in Au determined in this work fall between the thin-target data reported in Refs. 2 and 5. Very good agreement with the results given in Refs. 1, 14, and 16 has also been obtained for the stopping cross section in Ag. The energy spectra were measured for the bombarding energy E_{10} ranging from 0.4 (0.43) to 2.22 (2.09) MeV for the stopping element Au (Ag). Since the analyses were carried out for all the energy spectra from an $E_c \simeq E_{2B} - 0.1$ MeV to $E_{2B} = \alpha E_{10}$, the stopping cross section, generated from the determined parameters n, a, and z, is valid at least for $0.3 \leq E_\alpha \leq 2.0$ MeV. The plausibility of using these parameters in formula (7) in order to calculate the stopping cross section for α-particle energies outside the range has been discussed in detail in Refs. 2 and 3.

*Research supported in part by the National Science Foundation.

†Present address: Amoco Production Company, P. O. Box 50879, New Orleans, La.

[1]W. K. Chu and D. Powers, Phys. Rev. 187, 478 (1969).
[2]W. K. Lin, H. G. Olson, and D. Powers, Phys. Rev. B 8, 1881 (1973).
[3]W. K. Lin, H. G. Olson, and D. Powers, J. Appl. Phys. 44, 3631 (1973).
[4]W. A. Wenzel and W. Whaling, Phys. Rev. 87, 499 (1952).
[5]J. A. Borders, Radiat. Eff. 16, 253 (1972).
[6]U. Fano, Phys. Rev. 92, 328 (1953).
[7]F. T. Smith, R. P. Marchi, W. Aberth, D. C. Lorents, and O. Heinz, Phys. Rev. 161, 31 (1967).
[8]A. V. Wijngaarden, E. J. Brimner, and W. E. Baylis, Can. J. Phys. 48, 1835 (1970).
[9]C. W. Snyder, S. Rubin, W. A. Fowler, and C. C.

Lauritsen, Rev. Sci. Instrum. 21, 852 (1950).
[10]N. Bohr, K. Dan. Vidensk. Selsk. Mat.-Fys. Medd. 18, No. 8 (1948).
[11]J. M. Harris, W. K. Chu, and M-A. Nicolet, Thin Solid Films 19, 259 (1973).
[12]D. K. Brice, Phys. Rev. A 6, 1791 (1972).
[13]B. M. Shchigolev, in *Mathematical Analysis of Observations* (American Elsevier, New York, 1965), pp. 243–247.
[14]G. W. Gobeli, Phys. Rev. 103, 275 (1956), as tabulated by W. Whaling, in *Handbunch der Physik*, edited by S. Flügge (Springer-Verlag, Berlin, 1958), Vol. 34, p. 193.
[15]D. I. Porat and K. Ramavataram, Proc. Phys. Soc. Lond. 78, 1135 (1961).
[16]S. K. Allison and S. D. Warshaw, Rev. Mod. Phys. 25, 779 (1953) as tabulated by W. Whaling (cf. Ref. 14).